Parametric instability of the helical dynamo

Marine Peyrot[a] and Franck Plunian[b]
Laboratoire de Géophysique Interne et Tectonophysique, CNRS, Université Joseph Fourier, Maison des Géosciences, B.P. 53, 38041 Grenoble Cedex 9, France and Laboratoire des Ecoulements Géophysiques et Industriels, CNRS, Université Joseph Fourier, INPG, B.P. 53, 38041 Grenoble Cedex 9, France

Christiane Normand[c]
Service de Physique Théorique, CEA/DSM/SPhT, CNRS/URA 2306, CEA/Saclay, 91191 Gif-sur-Yvette Cedex, France

(Received 4 December 2006; accepted 3 April 2007; published online 30 May 2007)

We study the dynamo threshold of a helical flow made of a mean plus a fluctuating part. Two flow geometries are studied: (i) solid body and (ii) smooth. Two well-known resonant dynamo conditions, elaborated for stationary helical flows in the limit of large magnetic Reynolds numbers, are tested against lower magnetic Reynolds numbers and for fluctuating flows with zero mean. For a flow made of a mean plus a fluctuating part, the dynamo threshold depends on the frequency and the strength of the fluctuation. The resonant dynamo conditions applied on the fluctuating (respectively, mean) part seems to be a good diagnostic to predict the existence of a dynamo threshold when the fluctuation level is high (respectively, low). © *2007 American Institute of Physics*.
[DOI: 10.1063/1.2734118]

I. INTRODUCTION

In the context of recent dynamo experiments,[1–3] an important question is to identify the relevant physical parameters that control the dynamo threshold and eventually minimize it. In addition to the parameters usually considered, such as the geometry of the mean flow[4,5] or the magnetic boundary conditions,[6,7] the turbulent fluctuations of the flow seem to have an important influence on the dynamo threshold.[8–11] Some recent experimental results[12,13] suggest that the large spatial scales of these fluctuations could play a decisive role.

In this paper we consider a flow of large spatial scale, fluctuating periodically in time, such that its geometry at some given time is helical. Such helical flows have been identified to produce dynamo action.[14,15] Their efficiency has been studied in the context of fast dynamo theory[16–21] and they have led to the realization of several dynamo experiments.[3,22–24]

The dynamo mechanism of a helical dynamo is of stretch-diffuse type. The radial component B_r of the magnetic field is stretched to produce a helical field $(0, B_\theta, B_z)$, where (r, θ, z) are the cylindrical coordinates. The magnetic diffusion of the azimuthal component B_θ produces some radial component B_r due to the cylindrical geometry of the problem.[17] In this paper we shall consider two cases, depending on the type of flow shear necessary for the B_r stretching.

In case (i), the helical flow is solid body for $r<1$ and at rest for $r>1$ (the same conductivity is assumed in both domains). The flow shear is then infinite and localized at the discontinuity surface $r=1$. Gilbert[17] has shown that this dynamo is fast (positive growth rate in the limit of large magnetic Reynolds number) and is thus very efficient to generate a helical magnetic field of same pitch as the flow. In case (ii), the helical flow is continuous, and equal to zero for $r \geq 1$. The flow shear is then finite at any point. Gilbert[17] has shown that such a smooth helical flow is a slow dynamo and that the dynamo action is localized at a resonant layer $r=r_0$ such that $0<r_0<1$. Contrary to case (i), having a conducting external medium is not necessary here.

In both cases some resonant conditions leading to dynamo action have been derived.[16–18,20,21] Such resonant conditions can be achieved by choosing an appropriate geometry of the helical flow, such as changing its geometrical pitch. They have been derived for a stationary flow $\mathbf{U}(r,\theta,z)$ and can be generalized to a time-dependent flow of the form $\widetilde{\mathbf{U}}(r,\theta,z)\cdot f(t)$, where $f(t)$ is a periodic function of time. Now taking a flow composed of a mean part $\mathbf{U}$ plus a fluctuating part $\widetilde{\mathbf{U}}\cdot f(t)$, we expect the dynamo threshold to depend on the geometry of each part of the flow accordingly to the resonant condition of each of them and to the ratio of the intensities $|\widetilde{\mathbf{U}}|/|\mathbf{U}|$. However, we shall see that in some cases even a small intensity of the fluctuating part may have a drastic influence. The results also depend on the frequency of $f(t)$.

The Ponomarenko dynamo [case (i)] fluctuating periodically in time and with a fluctuation of infinitesimal magnitude had already been the object of a perturbative approach.[25] Here we consider a fluctuation of arbitrary magnitude. Comparing our results for a small fluctuation magnitude with those obtained with the perturbative approach, we found significant differences. We then realized that there was an error in the computation of the results published in Ref. 25 (though the perturbative development in itself is correct). In Appendix E, we give an erratum of these results.

[a]Electronic mail: Marine.Peyrot@ujf-grenoble.fr
[b]Electronic mail: Franck.Plunian@ujf-grenoble.fr
[c]Electronic mail: Christiane.Normand@cea.fr

II. MODEL

We consider a dimensionless flow defined in cylindrical coordinates (r,θ,z) by

$$\mathbf{U}=[0,r\Omega(r,t),V(r,t)]\cdot h(r)$$
$$\text{with } h(r)=\begin{cases}1, & r<1,\\ 0, & r>1,\end{cases} \tag{1}$$

corresponding to a helical flow in a cylindrical cavity which is infinite in the z direction, the external medium being at rest. Each component, azimuthal and vertical, of the dimensionless velocity is defined as the sum of a stationary part and of a fluctuating part:

$$\Omega(r,t)=[\bar{\mathrm{R}}_m+\tilde{\mathrm{R}}_m f(t)]\xi(r),$$
$$V(r,t)=[\bar{\mathrm{R}}_m\bar{\Gamma}+\tilde{\mathrm{R}}_m\tilde{\Gamma}f(t)]\zeta(r), \tag{2}$$

where $\bar{\mathrm{R}}_m$ and $\bar{\Gamma}$ ($\tilde{\mathrm{R}}_m$ and $\tilde{\Gamma}$) are the magnetic Reynolds number and a characteristic pitch of the stationary (fluctuating) part of the flow, respectively. In what follows we consider a fluctuation periodic in time, of the form $f(t)=\cos(\omega_f t)$. Depending on the radial profiles of the functions ξ and ζ, we determine two cases, (i) solid body and (ii) smooth flow, as

$$\text{(i):}\quad \xi=\zeta=1, \tag{3}$$

$$\text{(ii):}\quad \xi=1-r,\quad \zeta=1-r^2. \tag{4}$$

We note here that the magnetic Reynolds numbers are defined with the maximum angular velocity (either mean or fluctuating part) and the radius of the moving cylinder. Thinking of an experiment, it would not be sufficient to minimize the magnitude of the azimuthal flow. In particular, if $\bar{\Gamma}$ is large (considering a steady flow for simplicity), one would have to spend too many megawatts in forcing the z velocity. Therefore, the reader interested in linking our results to experiments should bear in mind that our magnetic Reynolds number is not totally adequate for it. A better definition of the magnetic Reynolds number might be, for example, $\hat{\mathrm{R}}_m=\bar{\mathrm{R}}_m\sqrt{1+\bar{\Gamma}^2}$. For a stationary flow of type (i), the minimum dynamo threshold $\hat{\mathrm{R}}_m$ is obtained for $\bar{\Gamma}=1.3$.

Both cases (i) and (ii) differ in the conductivity of the external medium $r>1$. In case (i), in which the magnetic generation occurs in a cylindrical layer in the neighborhood of $r=1$, a conducting external medium is necessary for dynamo action. For simplicity, we choose the same conductivity as the inner fluid. In the other hand, in case (ii), in which the magnetic generation is within the fluid, a conducting external medium is not necessary for dynamo action; thus, we choose an insulating external medium. Though the choice of the conductivity of the external medium is far from being insignificant for a dynamo experiment,[3,4,6,7] we expect that it does not change the overall meaning of the results given below.

We define the magnitude ratio of the fluctuation to the mean flow by $\rho=\tilde{\mathrm{R}}_m/\bar{\mathrm{R}}_m$. For $\rho=0$, there is no fluctuation and the dynamo threshold is given by $\bar{\mathrm{R}}_m$. On the other hand, for $\rho\gg 1$, the fluctuation dominates and the relevant quantity to determine the threshold is $\tilde{\mathrm{R}}_m=\rho\bar{\mathrm{R}}_m$. The perturbative approach of Normand[25] corresponds to $\rho\ll 1$.

The magnetic field must satisfy the induction equation

$$\frac{\partial\mathbf{B}}{\partial t}=\boldsymbol{\nabla}\times(\mathbf{U}\times\mathbf{B})+\nabla^2\mathbf{B}, \tag{5}$$

where the dimensionless time t is given in units of the magnetic diffusion time, implying that the flow frequency ω_f is also a dimensionless quantity. As the velocity does not depend on θ or on z, each magnetic mode in θ and z is independent from the others. Therefore, we can look for a solution of the form

$$\mathbf{B}(r,t)=\exp i(m\theta+kz)\mathbf{b}(r,t), \tag{6}$$

where m and k are the azimuthal and vertical wave numbers of the field, respectively. The solenoidality of the field $\boldsymbol{\nabla}\cdot\mathbf{B}=0$ then leads to

$$\frac{b_r}{r}+b_r'+i\frac{m}{r}b_\theta+ikb_z=0. \tag{7}$$

With the new variables $b^\pm=b_r\pm ib_\theta$, the induction equation can be written in the form

$$\frac{\partial b^\pm}{\partial t}+[k^2+i(m\Omega+kV)h(r)]b^\pm$$
$$=\pm\frac{i}{2}r\Omega' h(r)(b^+ +b^-)+\mathcal{L}^\pm b^\pm, \tag{8}$$

with

$$\mathcal{L}^\pm=\frac{\partial^2}{\partial r^2}+\frac{1}{r}\frac{\partial}{\partial r}-\frac{(m\pm 1)^2}{r^2}, \tag{9}$$

except in case (ii), where in the insulating external domain $(r>1)$, the induction equation takes the form

$$(\mathcal{L}^\pm-k^2)b^\pm=0. \tag{10}$$

At the interface $r=1$, both $\mathbf{B}$ and the z component of the electric field $\mathbf{E}=\boldsymbol{\nabla}\times\mathbf{B}-\mathbf{U}\times\mathbf{B}$ are continuous. The continuity of B_r and B_θ imply that of $b^\pm$. The continuity of $\mathbf{B}$ and (7) imply the continuity of b_r', which, combined with the continuity of E_z implies

$$[Db^\pm]_{1+}^{1-}\pm\frac{i\Omega_{r=1-}}{2}(b^+ +b^-)_{r=1}=0 \tag{11}$$

with $D=\partial/\partial r$ and $[h]_{1+}^{1-}=h_{(r=1-)}-h_{(r=1+)}$. We note that in case (ii), as $\Omega_{r=1-}=0$, (11) implies the continuity of $Db^\pm$ at $r=1$.

In summary, we calculate for both cases (i) and (ii) the growth rate

$$\gamma=\gamma(m,k,\bar{\Gamma},\tilde{\Gamma},\bar{\mathrm{R}}_m,\tilde{\mathrm{R}}_m,\omega_f) \tag{12}$$

of the kinematic dynamo problem and look for the dynamo

threshold (either $\bar{R}_m$ or $\tilde{R}_m$) such that the real part (Re γ) of γ is zero. In our numerical simulations we shall take $m=1$ for it leads to the lowest dynamo threshold.

A. Case (i): Solid body flow

In case (i), we set

$$m\Omega + kV = \bar{R}_m\bar{\mu} + \tilde{R}_m\tilde{\mu}f(t),$$
$$\text{with} \quad \bar{\mu} = m + k\bar{\Gamma} \quad \text{and} \quad \tilde{\mu} = m + k\tilde{\Gamma}, \tag{13}$$

and (8) changes into

$$\frac{\partial b^{\pm}}{\partial t} + \{k^2 + i[\bar{R}_m\bar{\mu} + \tilde{R}_m\tilde{\mu}f(t)]h(r)\}b^{\pm} = \mathcal{L}^{\pm}b^{\pm}. \tag{14}$$

For mathematical convenience, we take $\tilde{\mu}=0$. Thus, the nonstationary part of the velocity no longer occurs in (14). It occurs only in the expression of the boundary conditions (11) that can be written in the form

$$[Db^{\pm}]_{1+}^{1-} \pm \frac{i}{2}[\bar{R}_m + \tilde{R}_m f(t)](b^+ + b^-)_{r=1} = 0. \tag{15}$$

Taking $\tilde{\mu}=0$ corresponds to a pitch of the magnetic field equal to the pitch of the fluctuating part of the flow $-m/k = \tilde{\Gamma}$. On the other hand, it is not necessarily equal to the pitch of the mean flow (except if $\bar{\Gamma}=\tilde{\Gamma}$). In addition, we shall consider two situations depending on whether the mean flow is zero ($\bar{R}_m=0$) or not. The method used to solve Eqs. (14) and (15) is given in Appendix A.

At this stage we can make two remarks. First, according to boundary layer theory results[16,17] and for a stationary flow, in the limit of large $\bar{R}_m$, the magnetic field that has the highest growth rate satisfies $\bar{\mu}\approx 0$. This resonant condition means that the pitch of the magnetic field is roughly equal to the pitch of the flow. We shall see in Sec. III A that this stays true even at the dynamo threshold. Though the case of a fluctuating flow of type $\tilde{\mathbf{U}}\cdot f(t)$ may be more complex with possibly a skin effect, the resonant condition is presumably analogous; i.e., $\tilde{\mu}\approx 0$. This means that setting $\tilde{\mu}=0$ implies that if the fluctuations are sufficiently large ($\rho \gg 1$), dynamo action is always possible. This is indeed what will be found in our results. In other words, setting $\tilde{\mu}=0$, we cannot tackle the situation of a stationary dynamo flow to which a fluctuation acting against the dynamo would be added. This aspect will be studied with the smooth flow (ii).

Our second remark is about the effect of a phase lag between the azimuthal and vertical components of the flow fluctuation. Though we did not study the effect of an arbitrary phase lag, we can predict the effect of an out-of-phase lag. This would correspond to take a negative value of $\tilde{\Gamma}$. Solving numerically Eqs. (14) and (15) for the stationary flow and $m=1$, we find that dynamo action is possible only if $k\bar{\Gamma}<0$. For the fluctuating flow with zero mean, $m=1$ and $\tilde{\mu}=0$ necessarily imply that $k\tilde{\Gamma}=-1$. Let us now consider a flow containing both a stationary and a fluctuating part. Setting $\tilde{\Gamma}<0$ necessarily implies that $k>0$. For $\bar{\Gamma}>0$, the stationary flow, then, is not a dynamo. Therefore, in that case we expect the dynamo threshold to decrease for increasing ρ. For $\bar{\Gamma}<0$, together with $\tilde{\Gamma}<0$ and $k>0$, it is equivalent to take $\tilde{\Gamma}>0$ and $\bar{\Gamma}>0$ for $k<0$, and it is then covered by our subsequent results.

B. Case (ii): Smooth flow

For case (ii), we can directly apply the resonant condition made up for a stationary flow,[17,18] to the case of a fluctuating flow. For given m and k, the magnetic field is generated in a resonant layer $r=r_0$, where the magnetic field lines are aligned with the shear and thus minimize the magnetic field diffusion. This surface is determined by the following relation:[17,18]

$$m\Omega'(r_0) + kV'(r_0) = 0. \tag{16}$$

The resonant condition is satisfied if the resonant surface is embedded within the fluid:

$$0 < r_0 < 1. \tag{17}$$

As Ω and V depend on time, this condition may only be satisfied at discrete times. This implies successive periods of growth and damping, the dynamo threshold corresponding to a zero mean growth rate. We can also define two distinct resonant surfaces $\bar{r}_0$ and $\tilde{r}_0$ corresponding to the mean and fluctuating part of the flow:

$$m\bar{\Omega}'(\bar{r}_0) + k\bar{V}'(\bar{r}_0) = 0, \quad m\tilde{\Omega}'[\tilde{r}_0(t),t] + k\tilde{V}'[\tilde{r}_0(t),t] = 0, \tag{18}$$

with appropriate definitions of $\bar{\Omega},\bar{V},\tilde{\Omega}$ and $\tilde{V}$. In addition, if $\tilde{\Omega}$ and $\tilde{V}$ have the same time dependency, as in (2), then $\tilde{r}_0$ becomes time independent. We can then predict two different behaviors of the dynamo threshold versus the fluctuation rate $\rho=\tilde{R}_m/\bar{R}_m$. If $0<\bar{r}_0<1$ and $\tilde{r}_0>1$, then the dynamo threshold will increase with ρ. In this case, the fluctuation is harmful to dynamo action. On the other hand, if $0<\tilde{r}_0<1$, then the dynamo threshold will decrease with ρ.

From the definitions (18) and for a flow defined by (1), (2), and (4), we have

$$\bar{r}_0 = -(m/k)/(2\bar{\Gamma}) \quad \text{and} \quad \tilde{r}_0 = -(m/k)/(2\tilde{\Gamma}). \tag{19}$$

For $m=1$ and $k<0$, taking $\tilde{\Gamma}<0$ implies $\tilde{r}_0<0$ and then the impossibility of dynamo action for the fluctuating part of the flow. Therefore, we expect that the addition of a fluctuating flow with an out-of-phase lag between its vertical and azimuthal components will necessarily be harmful to dynamo action. This will be confirmed numerically in Sec. III C.

To solve (8), (10), and (11), we used a Galerkin approximation method in which the trial and weighting functions are chosen in such a way that the resolution of the induction equation is reduced to the conducting domain $r\leq 1$.[5] The method of resolution is given in Appendix D. For the time resolution we used a Runge-Kutta scheme of order 4.

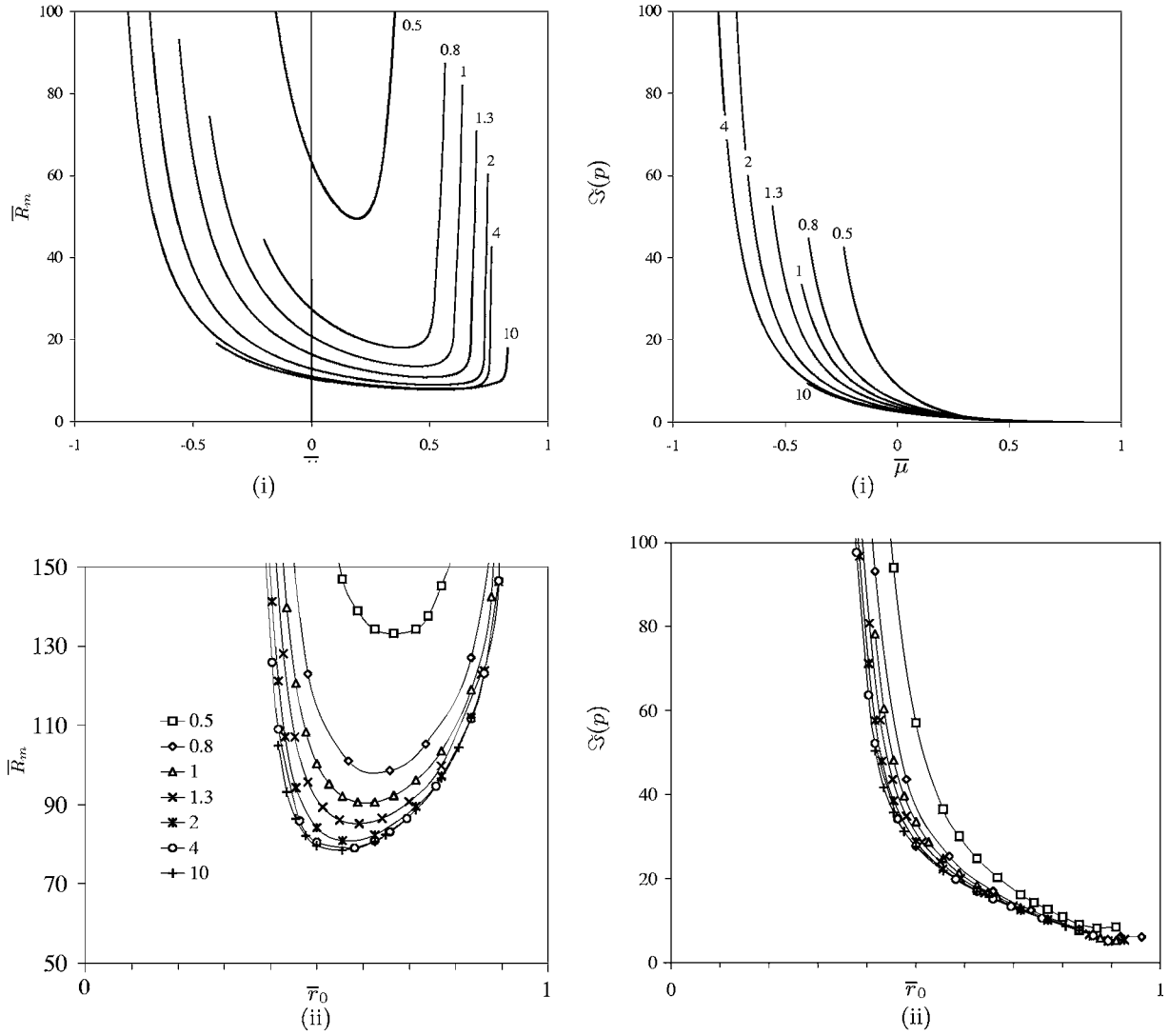

FIG. 1. The dynamo threshold $\bar{R}_m$ (left column) and Im (γ) (right column) versus (i) $\bar{\mu}$, (ii) $\bar{r}_0$, for the stationary case, $m=1$ and $\bar{\Gamma}=0.5$, 0.8, 1, 1.3, 2, 4, 10.

III. RESULTS

A. Stationary flow ($\tilde{R}_m=0$)

We solve

$$\text{Re } \gamma(m=1,\ k,\ \bar{\Gamma},\ 0,\ \bar{R}_m,\ 0,\ 0)=0 \tag{20}$$

with $k=(\bar{\mu}-1)/\bar{\Gamma}$ for case (i) and $k=-1/(2\bar{r}_0\bar{\Gamma})$ for case (ii). In case (i), the dispersion relation (A6) in Appendix A becomes $\mathcal{F}_0=0$. In Fig. 1, the threshold $\bar{R}_m$ and the field frequency Im (γ) are plotted versus $\bar{\mu}$ $(\bar{r}_0)$ for case (i) [(ii)], and for different values of $\bar{\Gamma}$. Though we do not know how these curves asymptote, and though the range of $\bar{\mu}$ $(\bar{r}_0)$ for which dynamo action occurs changes with $\bar{\Gamma}$, it is likely that the resonant condition $|\bar{\mu}|<1$ $(0<\bar{r}_0<1)$ is fulfilled for the range of $\bar{\Gamma}$ corresponding to a dynamo experiment ($\bar{\Gamma}\approx 1$).

B. Periodic flow with zero mean ($\bar{R}_m=0$)

We solve

$$\text{Re } \gamma(m=1,\ k,\ 0,\ \tilde{\Gamma},\ 0,\ \tilde{R}_m,\ \omega_f)=0. \tag{21}$$

In Fig. 2, the threshold $\tilde{R}_m$ is plotted versus ω_f for both cases (i) and (ii). In both cases we take $\tilde{\mu}=0$ corresponding to $k=-1/\tilde{\Gamma}$. For case (ii), it implies from (19) that $\tilde{r}_0=1/2$, meaning that the resonant surface is embedded in the fluid and thus favorable to dynamo action. In each case (i) $\tilde{\Gamma}=1,1.78$ and (ii) $\tilde{\Gamma}=1,2$, we observe two regimes: one at low frequencies for which the threshold does not depend on ω_f and the other at high frequencies for which the threshold behaves like $\tilde{R}_m\propto\omega_f^{3/4}$.

To understand the existence of these two regimes, we pay attention to the time evolution of the magnetic field for

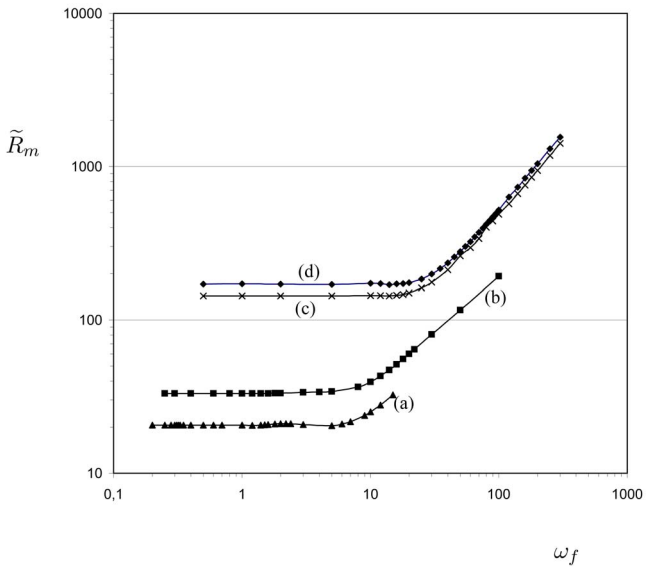

FIG. 2. Dynamo threshold $\widetilde{\mathrm{R}}_m$ versus ω_f for case (i) with $\widetilde{\mu}=0$ and (a) $\widetilde{\Gamma}=1.78$, and (b) $\widetilde{\Gamma}=1$; for case (ii) with $\tilde{r}_0=0.5$, (c) $\widetilde{\Gamma}=2$, and (d) $\widetilde{\Gamma}=1$.

different frequencies ω_f. In Fig. 3, the time evolution of b^- (real and imaginary parts) for case (ii) $\widetilde{\Gamma}=1$ [case (d) in Fig. 2] is plotted for several frequencies ω_f.

1. Low frequency regime

For low frequencies ($\omega_f=1$), we observe two time scales: periodic phases of growth and decrease of the field, with a time scale equal to the period of the flow as expected by Floquet's theory. In addition, the field has an eigenfrequency much higher than ω_f. In fact, the slow phases of growth and decrease seem to occur every half-period of the flow. This can be understood from the following remarks.

First of all, the growth (or decrease) of the field does not depend on the sign of the flow. Indeed, from (8), we show that if $b^{\pm}(m,k)$ is a solution for (Ω, V), then its complex conjugate $b^{\pm *}(m,k)$ is a solution for $(-\Omega, -V)$. Therefore, we have $b^{\pm}(t+T/2)=b^{\pm *}(t)$, where $T=2\pi/\omega_f$ is the period of the flow. Now from Floquet's theory (see Appendix A), we may write $\mathbf{b}(r,t)$ of the form $\mathbf{b}(r,\tau)\exp(\gamma t)$, with $\mathbf{b}(r,\tau)$ 2π-periodic in $\tau=\omega_f t$. This implies that changing (Ω, V) in $(-\Omega, -V)$ changes the sign of Im (γ). This is consistent with the fact that for given m and k, the direction of propagation of **B** changes with the direction of the flow. Therefore changing the sign of the flow changes the sign of propagation of the field but does not change the magnetic energy, neither the dynamo threshold $\widetilde{\mathrm{R}}_m$, which are then identical from one half-period of the flow to another. This means that the dynamo threshold does not change if we consider $f(t)=|\cos(\omega_f t)|$ instead of $\cos(\omega_f t)$. It is then sufficient to concentrate on one half-period of the flow, such as, for example $[\pi/2\omega_f, 3\pi/2\omega_f]$ (modulo π).

The second remark uses the fact that the flow geometry that we consider does not change in time (only the flow magnitude changes). For such a geometry we can calculate the dynamo threshold $\bar{\mathrm{R}}_m$ corresponding to the stationary case. Coming back to the fluctuating flow, we then understand that $\widetilde{\mathrm{R}}_m|f(t)|>\bar{\mathrm{R}}_m$ $[\widetilde{\mathrm{R}}_m|f(t)|<\bar{\mathrm{R}}_m]$ corresponds to a growing (decreasing) phase of the field. Assuming that the dynamo threshold $\widetilde{\mathrm{R}}_m$ is given by the time average $\langle\cdot\rangle$ of the flow magnitude leads to the following estimation for $\widetilde{\mathrm{R}}_m$:

$$\widetilde{\mathrm{R}}_m \approx \frac{\pi}{2}\bar{\mathrm{R}}_m \tag{22}$$

as $\langle|\cos(\omega_f t)|\rangle=2/\pi$. For the four cases (a), (b), (c), and (d) in Fig. 2, we give in Table I the ratio $2\widetilde{\mathrm{R}}_m/\pi\bar{\mathrm{R}}_m$, which is found to be always close to unity. In this interpretation of the results, the frequency ω_f does not appear, provided that it is sufficiently weak in order that the successive phases of growth and decrease have sufficient time to occur. This can explain why for low frequencies in Fig. 2, the dynamo threshold $\widetilde{\mathrm{R}}_m$ does not depend on ω_f.

Finally the frequencies $\bar{\omega}$ of the stationary case for $\bar{\Gamma}=\widetilde{\Gamma}$ are also reported in Table I. For a geometry identical to case (d), we find, in the stationary case, $\bar{\omega}=33$, which indeed corresponds to the eigenfrequency of the field occurring in Fig. 3 for $\omega_f=1$. The previous remarks assume that the flow frequency is sufficiently small compared to the eigenfrequency of the field, in order to have successive phases of growth and decrease of the field. We can check that the values of $\bar{\omega}$ given in Table I are indeed reasonable estimations of the transition frequencies between the low and high frequency regimes in Fig. 2.

2. High frequency regime

In case (ii) and for high frequencies (Fig. 3, $\omega_f=100$), the signal is made of harmonics without growing or decreasing phases. We note that the eigenfrequencies of the real and imaginary parts of b^- are different, the one being twice the other.

In case (i), relying on the resolution of Eqs. (14) and (15) given in Appendix A, we can show that $\widetilde{\mathrm{R}}_m \propto \omega_f^{3/4}$. We also find that some double frequency as found in Fig. 3 for case (ii) can emerge from an approximate 3×3 matrix system. As these developments necessitate the notations introduced in Appendix A, they are postponed until Appendix B.

3. Further comments about the ability for fluctuating flows to sustain dynamo action

We found and explained how a fluctuating flow (zero mean) can act as a dynamo. We also understood why the dynamo threshold for a fluctuating flow is higher than that for a stationary flow with the same geometry. It is because the time-average of the velocity norm of the fluctuating flow is on the mean lower than that of the stationary flow. This can be compensated with other definitions of the magnetic Reynolds number. Our definition is based on $\max_t|\Omega(r,t)|$. Another definition based on $\langle|\Omega(r,t)|\rangle_t$ would exactly compensate the difference.

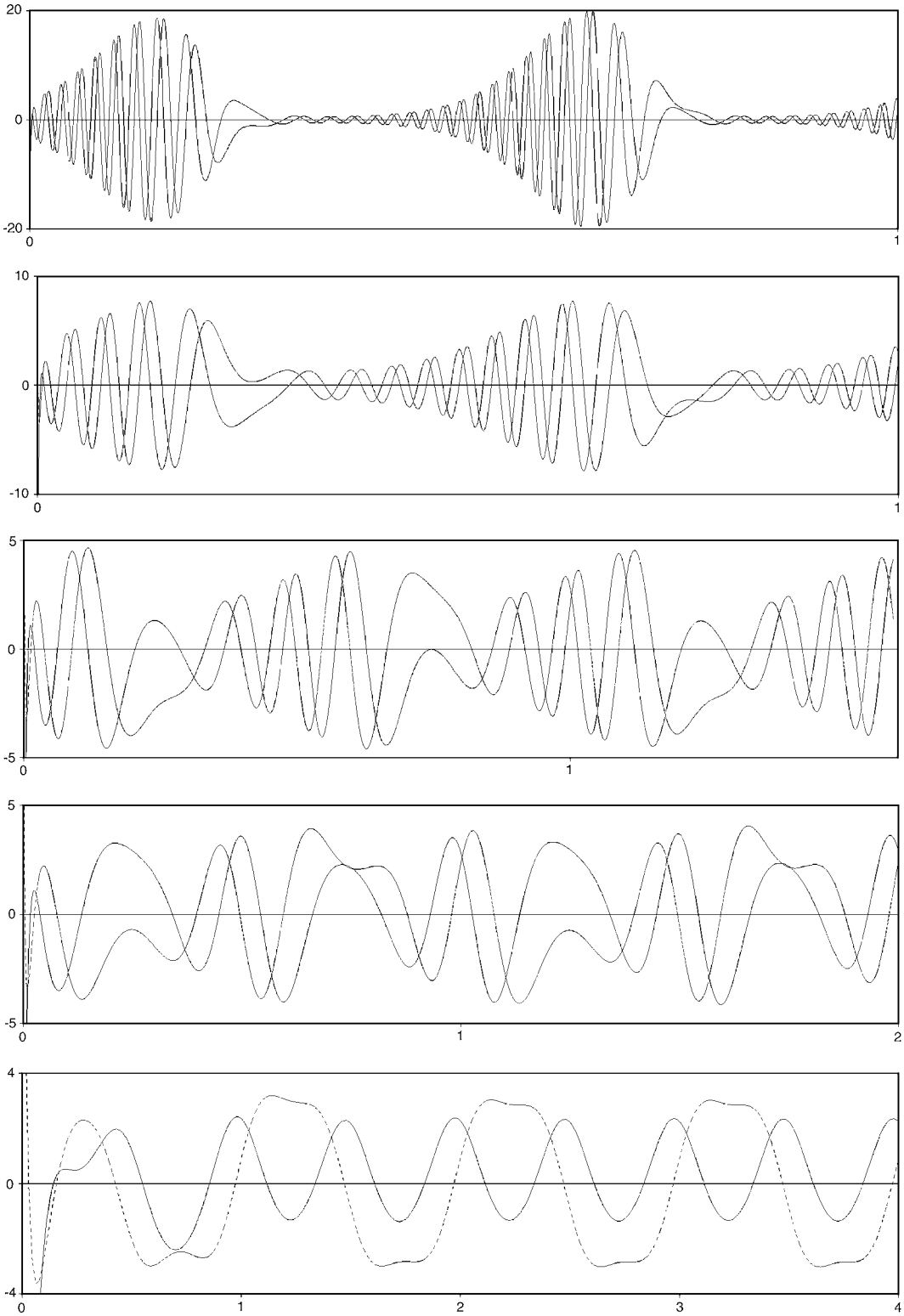

FIG. 3. Time evolution of Re(b^-) (solid lines) and Im(b^-) (dotted lines) for several values of ω_f (from top to bottom ω_f=1; 2, 5, 10, 100), for case (ii) with $\tilde{\Gamma}$=1. Time unity corresponds here to $2\pi/\omega_f$.

Recently, a controversy appeared about the difficulty for a fluctuating flow (zero mean) to sustain dynamo action at low P_m,[26] whereas a mean flow (nonzero time average) exhibits a finite threshold at low P_m[10,27] (the magnetic Prandtl number P_m being defined as the ratio of the viscosity to the diffusivity of the fluid). This issue is important not only for dynamo experiments but also for natural objects such as the Earth's inner core or the solar convective zone in which the electroconducting fluid is characterized by a low P_m. Though we did not study this problem, our results suggest that the dynamo threshold should not be much different between fluctuating and mean flows, provided an appropriate defini-

TABLE I. Dynamo thresholds $\tilde{R}_m$ for a fluctuating flow at low frequency, $\bar{R}_m$ (and $\bar{\omega}$) for a stationary flow with the same geometry. The labels (a)–(d) have the same meaning as in Fig. 2.

	$\tilde{R}_m$	$\bar{R}_m$	$2\tilde{R}_m/\pi\bar{R}_m$	$\bar{\omega}$
(a)	21	13	1.03	4.4
(b)	33	21	1	3.1
(c)	143	84	1.08	28.8
(d)	170	100	1.08	33

tion of the magnetic Reynolds number is taken. In that case, why does it seem so difficult to sustain dynamo action at low P_m for a fluctuating flow,[26] whereas it seems much easier for a mean flow?[10,27]

In the simulations with a mean flow,[10,27] two dynamo regimes have been found, one with a threshold much lower than the other. In the lowest threshold regime, the magnetic field is generated at some infinite scale in two directions.[27] There is then an infinite scale separation between the magnetic and the velocity field, and the dynamo action is probably of mean-field type and might be understood in terms of α-effect, β-effect, etc. In that case, removing the periodic boundary conditions would cancel the scale separation and imply the loss of the dynamo action. In the highest threshold regime, the magnetic field is generated at a scale similar to the flow scale, the periodic boundary conditions are forgotten and the dynamo action can no longer be understood in terms of an α-effect. In order to compare the mean flow results[27] with those for a fluctuating flow,[26] we have to consider only the highest threshold regime in Ref. 27, the lowest one relying on mean-field dynamo processes due to the periodic boundary conditions and which are absent in the fluctuating flow calculations.[26]

Now when comparing the threshold of the highest threshold regime for a mean flow with the threshold obtained for a fluctuating flow and with appropriate definitions of R_m, a strong difference remains at low P_m. A speculation made by Schekochihin *et al.*[28] is that the highest threshold regime obtained for the mean flow at low P_m would correspond in fact to the large P_m results for the fluctuating flow. Their arguments rely on the fact that the mean flow in Ref. 27 is peaked at large scale and is thus spatially smooth for the generated magnetic field. It would then belong to the same class as the large-P_m fluctuation dynamo. Both dynamo thresholds are found to be similar indeed, and thus the discrepancy vanishes.

Though the helical flow that we consider here is noticeably different (no chaotic trajectories) it may have some consistency with the simulations at large P_m mentioned above and at least supports the speculation by Schekochihin *et al.*[28]

C. Periodic flow with nonzero mean

We are now interested in the case in which both $\tilde{R}_m \neq 0$ and $\bar{R}_m \neq 0$. The flow is then the sum of a nonzero mean part and a fluctuating part. We have considered two approaches depending on which part of the flow geometry is fixed, either the mean or the fluctuating part.

1. $\bar{\Gamma}=1$

Here we fix $\bar{\Gamma}=1$, $m=1$, and $k=-1$, and vary $\tilde{\Gamma}$, ρ, and ω_f for case (ii). We then solve the equation

$$\mathrm{Re}\ \gamma(m=1,\ k=-1,\ \bar{\Gamma}=1,\ \tilde{\Gamma}=1/2\tilde{r}_0,\ \bar{R}_m,\ \tilde{R}_m=\rho\bar{R}_m,\ \omega_f)=0 \tag{23}$$

to plot $\bar{R}_m$ as a function of ρ in Fig. 4 for values of $\tilde{r}_0$ and ω_f. From (19), we have $\bar{r}_0=1/2$, which corresponds to a mean flow geometry with a dynamo threshold about 100. The curves are plotted for several values of $\tilde{\Gamma}$ leading to values of $\tilde{r}_0$ not necessarily between 0 and 1. We consider two fluctua-

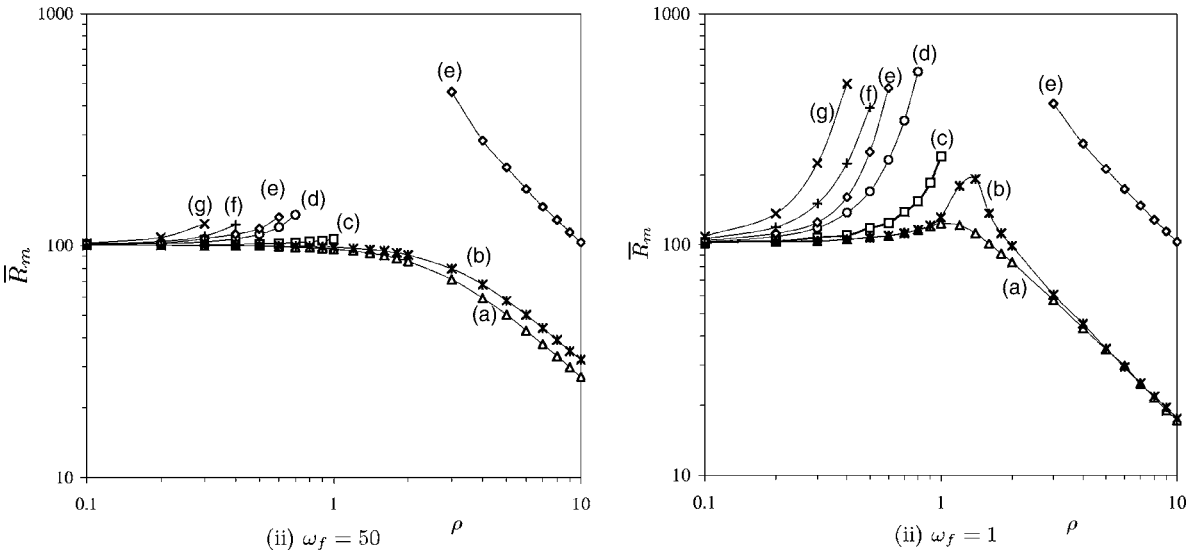

FIG. 4. Dynamo threshold $\bar{R}_m$ versus ρ for case (ii), for two frequencies $\omega_f=50$ and $\omega_f=1$ and $\bar{r}_0=1/2$ ($\bar{\Gamma}=1$, $m=1$, $k=-1$). The different curves correspond to $\tilde{r}_0$= (a) 1/2; (b) 2/3; (c) 1; (d) ∞; (e) 1/4; (f) −1; (g) −1/2 [$\tilde{\Gamma}$= (a) 1; (b) 0.75; (c) 0.5; (d) 0; (e) 2; (f) −0.5; (g) −1].

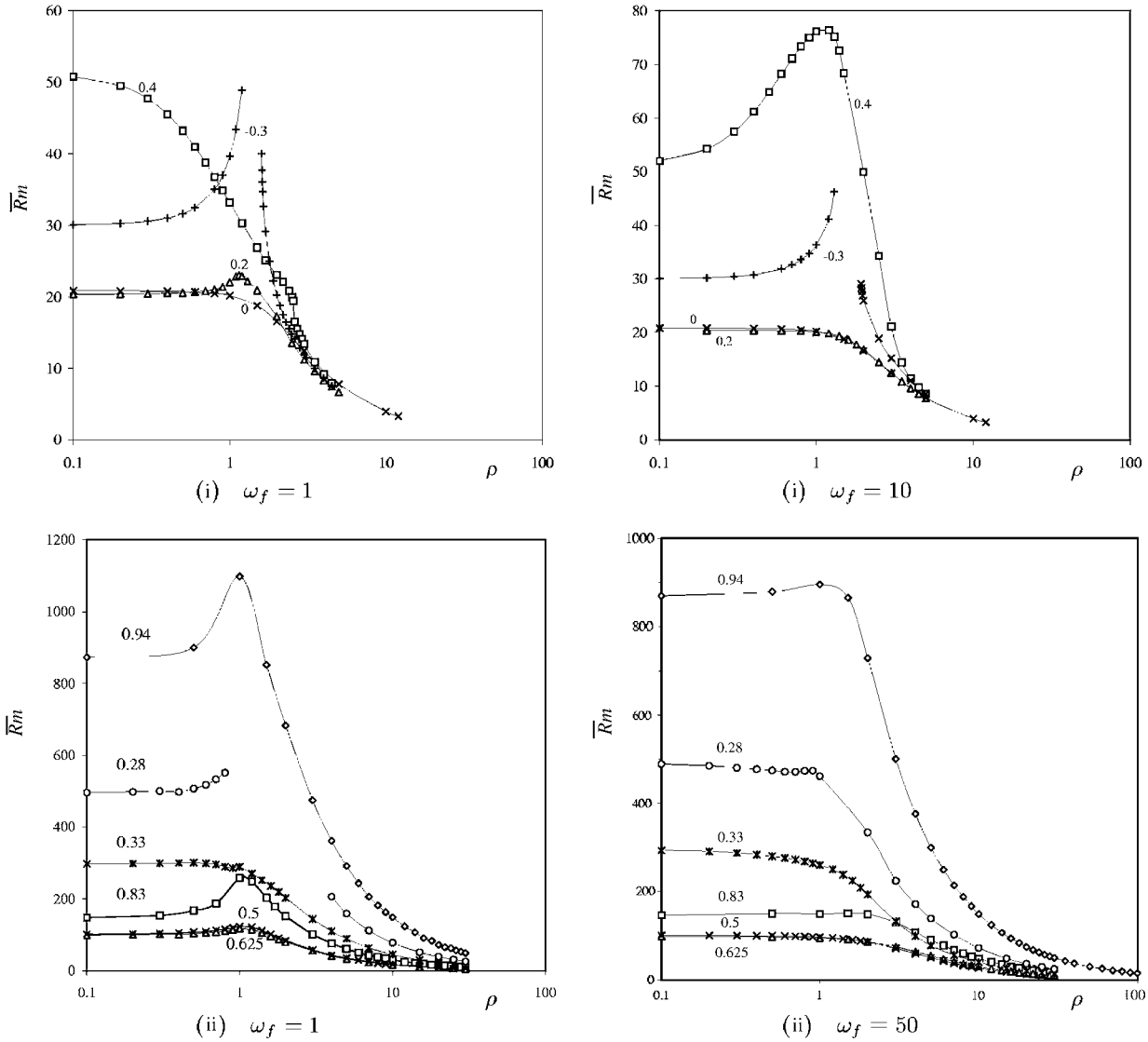

FIG. 5. The dynamo threshold $\bar{R}_m$ versus ρ for $k=-1$, $m=1$, and $\tilde{\Gamma}=1$ [$\tilde{\mu}=0$ in case (i) and $\tilde{r}_0=0.5$ in case (ii)] and $\omega_f=1$, 10, or 50. The labels correspond to $\bar{\mu}$ in case (i) and $\bar{r}_0$ in case (ii).

tion frequencies $\omega_f=1$ and $\omega_f=50$. We find that the dynamo threshold $\bar{R}_m$ increases asymptotically with ρ unless the resonant condition $0<\tilde{r}_0<1$ is satisfied; see curves (a), (b), and (e). For these three curves we checked that in the limit of large ρ, $\bar{R}_m=O(\rho^{-1})$. For $\tilde{r}_0=1/4$ [curve (e)] and for $\rho\approx 1$ we do not know if a dynamo threshold exists.

2. $\tilde{\Gamma}=1$

Here we fix $\tilde{\Gamma}=1$, $m=1$, and $k=-1$ and vary $\bar{\Gamma}$, ρ, and ω_f. We then solve the equation

$$\mathrm{Re}\ \gamma(m=1,\ k=-1,\ \bar{\Gamma},\ \tilde{\Gamma},\ \bar{R}_m,\ \tilde{R}_m=\rho\bar{R}_m,\ \omega_f)=0 \quad (24)$$

with $\bar{\Gamma}=1-\bar{\mu}$ in case (i) and $\bar{\Gamma}=1/2\bar{r}_0$ in case (ii). In Fig. 5, $\bar{R}_m$ is plotted versus ρ for values of $\bar{\mu}$ ($\bar{r}_0$) in case (i) [(ii)] and ω_f. Taking $\tilde{\Gamma}=1$, $m=1$, and $k=-1$ implies $\tilde{\mu}=0$ in case (i) and $\tilde{r}_0=0.5$ in case (ii). In both cases (i) and (ii) the fluctuating part of the flow satisfies the resonant condition for which dynamo action is possible. This implies that $\bar{R}_m$ should scale as $O(\rho^{-1})$ provided that ρ is sufficiently large. In each case we consider two flow frequencies $\omega_f=1$ and $\omega_f=10$ for case (i); $\omega_f=1$ and $\omega_f=50$ for case (ii). The curves are plotted for different values of $\bar{\Gamma}$ corresponding to $|\bar{\mu}|<1$ for case (i) and $0<\bar{r}_0<1$ for case (ii). For large ρ, we checked that $\bar{R}_m=O(\rho^{-1})$. The main difference between the curves is that $\bar{R}_m$ versus ρ may decrease monotonically or not. In particular, in case (i) for $\bar{\mu}=0.4$, $\bar{R}_m$ decreases by 40% when ρ goes from 0 to 1 showing that even a small fluctuation can strongly decrease the dynamo threshold. In most of the curves there is a bump for ρ around unity showing a strong increase of the threshold before the final decrease at larger ρ.

3. $\bar{\Gamma}=\tilde{\Gamma}=1$

Here we fix $\bar{\Gamma}=\tilde{\Gamma}=1$, $m=1$, and $k=-1$ for the case (ii) and vary ω_f and ρ. We then solve the equation

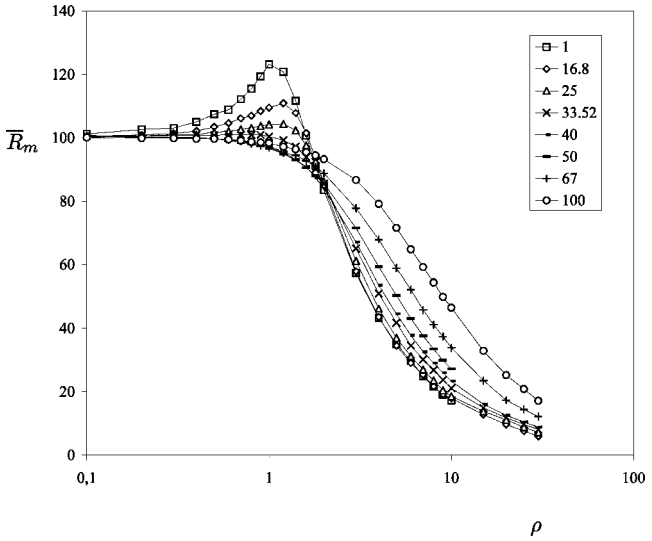

FIG. 6. Dynamo threshold $\bar{\mathrm{R}}_m$ versus ρ for $\bar{r}_0=\tilde{r}_0=0.5$ ($\bar{\Gamma}=\tilde{\Gamma}=1$). The labels correspond to different values of ω_f. The eigenfrequency for $\rho=0$ is $\bar{\omega}=33$.

$$\mathrm{Re}\ \gamma(m=1,\ k=-1,\ \bar{\Gamma}=1,\ \tilde{\Gamma}=1,\ \bar{\mathrm{R}}_m,\ \tilde{\mathrm{R}}_m=\rho\bar{\mathrm{R}}_m,\ \omega_f)=0 \tag{25}$$

to plot $\bar{\mathrm{R}}_m$ versus ρ in Fig. 6 for various frequencies ω_f. Taking $\bar{\Gamma}=\tilde{\Gamma}=1$, $m=1$, and $k=-1$ implies $\bar{r}_0=\tilde{r}_0=0.5$. For ρ larger than 1, $\bar{\mathrm{R}}_m$ decreases as $O(\rho^{-1})$ as mentioned earlier. For ρ smaller than unity, $\bar{\mathrm{R}}_m$ decreases versus ρ monotonically only if ω_f is large enough. In fact the transition value of ω_f, above which $\bar{\mathrm{R}}_m$ decreases monotonically is exactly the field frequency $\bar{\omega}$ (here, $\bar{\omega}=33$) corresponding to $\rho=0$. This shows that a fluctuation of small intensity ($\rho\leq 1$) helps the dynamo action only if its frequency is sufficiently high. This is shown in Appendix C for case (i). However, the frequency above which a small fluctuation intensity helps the dynamo may be much larger than $\bar{\omega}$. For example, in case (i) for $\bar{\mu}=0.4$ and $\tilde{\mu}=0$ represented in Fig. 5, we have $\bar{\omega}=0.51$. For $\omega_f=1$ small fluctuation helps, for $\omega_f=10$ they do not help, and for higher frequencies they help again.

IV. DISCUSSION

In this paper we studied the modification of the dynamo threshold of a stationary helical flow by the addition of a large scale helical fluctuation. We extended a previous asymptotic study[25] to the case of a fluctuation of arbitrary intensity (controlled by the parameter ρ). We knew from previous studies[17,18] that the dynamo efficiency of a helical flow is characterized by some resonant condition at large R_m. First we verified numerically that such resonant condition holds at lower R_m corresponding to the dynamo threshold, for both a stationary and a fluctuating (no mean) helical flow. For a helical flow made of a mean part plus a fluctuating part we showed that, in the asymptotic cases $\rho\ll 1$ (dominating mean) and $\rho\gg 1$ (dominating fluctuation), it is naturally the resonant condition of the mean (for the first case) or the fluctuating (for the second case) part of the flow that governs the dynamo efficiency and then the dynamo threshold. In between, for ρ of order unity and if the resonant condition of each flow part (mean and fluctuating) is satisfied, the threshold first increases with ρ before reaching an asymptotic behavior in $O(\rho^{-1})$. However, there is no systematic behavior as depicted in Fig. 5, case (i), for $\omega_f=1$ and $\bar{\mu}=0.4$, in which a threshold decrease of 40% is obtained between $\rho=0$ and $\rho=1$. If the fluctuation part of the flow does not satisfy the resonant condition, then the dynamo threshold increases drastically with ρ.

Contrary to the case of a cellular flow,[11] there is no systematic effect of the phase lag between the different components of the helical flow. For the helical flow geometry it may imply an increase or a decrease of the dynamo threshold, depending how it changes the resonant condition mentioned above.

There is some similarity between our results and those obtained for a noisy (instead of periodic) fluctuation.[8] In particular, in Ref. 8 it was found that increasing the noise level the threshold first increases due to geometrical effects of the magnetic field lines and then decreases at larger noise. This could explain why at $\rho\approx 1$ we generally obtain a maximum of the dynamo threshold.

Finally, these results show that the optimization of a dynamo experiment depends not only on the mean part of the flow but also on its nonstationary large scale part. If the fluctuation is not optimized then the threshold may increase drastically with (even small) ρ, ruling out any hope of producing dynamo action. In addition, even if the fluctuation is optimized (resonant condition satisfied by the fluctuation), our results suggest that there is generally some increase of the dynamo threshold with ρ when $\rho\leq 1$. If the geometry of the fluctuation is identical to that of the mean part of the flow, there can be some slight decrease of the threshold at high frequencies but this decrease is rather small. When $\rho>1$, the dynamo threshold decreases as $O(\rho^{-1})$, which at first sight seems interesting. However, we have to keep in mind that as soon as $\rho>1$, the driving power spent to maintain the fluctuation is larger than that to maintain the mean flow. The relevant dynamo threshold is, then, no longer $\bar{\mathrm{R}}_m$, but $\tilde{\mathrm{R}}_m=\rho\bar{\mathrm{R}}_m$ instead. In addition monitoring large scale fluctuations in an experiment may not always be possible, especially if they occur from flow destabilization. In that case it is better to try cancelling them as was done in the von Karman sodium experiment in which an azimuthal belt has been added.[29]

ACKNOWLEDGMENTS

We acknowledge B. Dubrulle, F. Pétrélis, R. Stepanov, and A. Gilbert for fruitful discussions.

APPENDIX A: RESOLUTION OF EQS. (14) AND (15) FOR CASE (I): SOLID BODY FLOW

As $f(t)$ is time-periodic of period $2\pi/\omega_f$, we look for $\mathbf{b}(r,t)$ in the form $\mathbf{b}(r,\tau)\exp(\gamma t)$ with $\mathbf{b}(r,\tau)$ being 2π-periodic in $\tau=\omega_f t$. Thus, we look for the functions $b^{\pm}(r,\tau)$ in the form

$$b^{\pm}(r,\tau) = \sum b_n^{\pm}(r)\exp(in\tau) \tag{A1}$$

where, from (14) and for $\tilde{\bar{\mu}}=0$, the Fourier coefficients $b_n^{\pm}(r)$ must satisfy

$$\{\gamma + k^2 + i[\bar{\mathrm{R}}_m\bar{\mu}h(r) + n\omega_f]\}b_n^{\pm} = \mathcal{L}^{\pm}b_n^{\pm}. \tag{A2}$$

In addition, the boundary condition (15) with $f(t)=\cos(\tau)$ implies

$$[Db_n^{\pm}]_{1+}^{1-} \pm \frac{i}{2}\bar{\mathrm{R}}_m(b_n^{+} + b_n^{-})_{r=1}$$

$$\pm \frac{i}{4}\tilde{\bar{\mathrm{R}}}_m(b_{n-1}^{+} + b_{n-1}^{-} + b_{n+1}^{+} + b_{n+1}^{-})_{r=1} = 0. \tag{A3}$$

The solutions of (A2), which are continuous at $r=1$, can be written in the form

$$b_n^{\pm} = C_n^{\pm}\psi_n^{\pm}, \quad \text{with } \psi_n^{\pm} = \begin{cases} I^{\pm}(q_n r)/I^{\pm}(q_n), & r<1, \\ K^{\pm}(s_n r)/K^{\pm}(s_n), & r>1, \end{cases} \tag{A4}$$

with

$$q_n^2 = k^2 + \gamma + i(\bar{\mathrm{R}}_m\bar{\mu} + n\omega_f), \quad s_n^2 = k^2 + \gamma + in\omega_f. \tag{A5}$$

Substituting (A4) in (A3), we obtain the following system:

$$C_n^{\pm}\mathcal{R}_n^{\pm} \pm i\frac{\bar{\mathrm{R}}_m}{2}(C_n^{+} + C_n^{-}) \pm i\frac{\tilde{\bar{\mathrm{R}}}_m}{4}(C_{n-1}^{+} + C_{n-1}^{-} + C_{n+1}^{+} + C_{n+1}^{-}) = 0 \tag{A6}$$

with $\mathcal{R}_n^{\pm} = q_n I_n^{\pm\prime}/I_n^{\pm} - s_n K_n^{\prime\pm}/K_n^{\pm}$ and where $I_n^{\pm} = I_{m\pm1}(q_n)$ and $K_n^{\pm} = K_{m\pm1}(s_n)$ are modified Bessel functions of first and second kind.

The system (A6) implies the following matrix dispersion relation:

$$\mathcal{F}_n C_n - i\frac{\tilde{\bar{\mathrm{R}}}_m}{4}(\mathcal{R}_n^{+} - \mathcal{R}_n^{-})(C_{n-1} + C_{n+1}) = 0 \tag{A7}$$

with $C_j = C_j^{+} + C_j^{-}$ and

$$\mathcal{F}_n = \mathcal{R}_n^{+}\mathcal{R}_n^{-} - i(\bar{\mathrm{R}}_m/2)(\mathcal{R}_n^{+} - \mathcal{R}_n^{-}). \tag{A8}$$

Solving the system (A7) is equivalent to setting to zero the determinant of the matrix A defined by

$$A_{nn} = \mathcal{F}_n, A_{n\,n-1} = A_{n\,n+1} = -i\frac{\tilde{\bar{\mathrm{R}}}_m}{4}(\mathcal{R}_n^{+} - \mathcal{R}_n^{-}) \tag{A9}$$

and with all other coefficients being set to zero.

APPENDIX B: HIGH FREQUENCY REGIME FOR THE PERIODIC FLOW (I) WITH ZERO MEAN

Following the notation of Appendix A, and considering a periodic flow (i) with zero mean, we have $\bar{\mu}=0$. From (A5) this implies that $q_n=s_n$. Using the identity

$$I_n^{\pm\prime}K_n^{\pm} - K_n^{\prime\pm}I_n^{\pm} = \frac{1}{s_n}, \tag{B1}$$

we obtain $\mathcal{R}_n^{\pm} = (I_n^{\pm}K_n^{\pm})^{-1}$. As $\bar{\mathrm{R}}_m=0$, Eq. (A8) becomes $\mathcal{F}_n = \mathcal{R}_n^{+}\mathcal{R}_n^{-}$. We can then rewrite the system (A7) in the form

$$C_n + i\frac{\tilde{\bar{\mathrm{R}}}_m}{4}(I_n^{+}K_n^{+} - I_n^{-}K_n^{-})(C_{n-1} + C_{n+1}) = 0. \tag{B2}$$

From the asymptotic behavior of the Bessel functions for high arguments, we have

$$\alpha_n \equiv I_n^{-}K_n^{-} - I_n^{+}K_n^{+} \approx 1/s_n^3. \tag{B3}$$

For the high values of n, these terms are negligible and in first approximation we keep in the system (B2) only the terms corresponding to $n=0,\pm1$. This leads to a 3×3 matrix system whose determinant is

$$1 + \frac{(\tilde{\bar{\mathrm{R}}}_m)^2}{16}\alpha_0(\alpha_{-1} + \alpha_1) = 0. \tag{B4}$$

At high forcing frequencies ω_f, we have $s_{\pm1} \approx \sqrt{\omega_f}$. Together with (B4), it implies

$$\tilde{\bar{\mathrm{R}}}_m \approx \omega_f^{3/4}. \tag{B5}$$

In addition, from the approximate 3×3 matrix system, the double-frequency $2\omega_f$ depicted in Fig. 3 emerges for $n=\pm1$.

APPENDIX C: HIGH FREQUENCY REGIME AND SMALL MODULATION AMPLITUDE FOR THE PERIODIC FLOW (I) WITH NONZERO MEAN

For small amplitude modulation $\rho\ll1$, the system (A6) is truncated so as to keep the first Fourier modes $n=0$ and $n=\pm1$. The dispersion relation

$$\mathcal{F}_0 + \rho^2\left(\frac{\bar{\mathrm{R}}_m}{4}\right)^2(\mathcal{R}_0^{+} - \mathcal{R}_0^{-})\left(\frac{\mathcal{R}_{-1}^{+} - \mathcal{R}_{-1}^{-}}{\mathcal{F}_{-1}} + \frac{\mathcal{R}_{+1}^{+} - \mathcal{R}_{+1}^{-}}{\mathcal{F}_{+1}}\right) = 0 \tag{C1}$$

is then solved perturbatively setting $\bar{\mathrm{R}}_m = \mathrm{R}_0 + \delta\mathrm{R}$ and $\bar{\omega} = \omega_0 + \delta\omega$ and expanding $\mathcal{F}_0(\bar{\mathrm{R}}_m, \bar{\omega})$ to first order in $\delta\mathrm{R}$ and $\delta\omega$ given that $\mathcal{F}_0(\mathrm{R}_0, \omega_0)=0$ and with the constants $C_0^{\mp} = \pm\mathcal{R}_0^{\pm}$. The dispersion relation (C1) becomes

$$\delta\mathrm{R}\frac{\partial\mathcal{F}_0}{\partial\bar{\mathrm{R}}_m} + \delta\omega\frac{\partial\mathcal{F}_0}{\partial\bar{\omega}} = -\rho^2\left(\frac{\mathrm{R}_0}{4}\right)^2 C_0\left(\frac{\beta_{-1}}{\mathcal{F}_{-1}} + \frac{\beta_{+1}}{\mathcal{F}_{+1}}\right) \tag{C2}$$

with $\beta_n = \mathcal{R}_n^{+} - \mathcal{R}_n^{-}$. The threshold and frequency shifts that behave like ρ^2 are written $\delta\mathrm{R} = \rho^2\mathrm{R}_2$ and $\delta\omega = \rho^2\omega_2$. In the left-hand side of (C2) the partial derivatives are given by

$$\frac{\partial\mathcal{F}_0}{\partial\bar{\omega}} = -\frac{1}{C_0}\left[(C_0^{+})^2\frac{\partial\mathcal{R}_0^{+}}{\partial\bar{\omega}} - (C_0^{-})^2\frac{\partial\mathcal{R}_0^{-}}{\partial\bar{\omega}}\right], \tag{C3}$$

$$\frac{\partial\mathcal{F}_0}{\partial\bar{\mathrm{R}}_m} = -\frac{1}{C_0}\left[(C_0^{+})^2\frac{\partial\mathcal{R}_0^{+}}{\partial\bar{\mathrm{R}}_m} - (C_0^{-})^2\frac{\partial\mathcal{R}_0^{-}}{\partial\bar{\mathrm{R}}_m}\right] - \frac{i}{2}C_0. \tag{C4}$$

One can show that the partial derivatives of $\mathcal{R}_0^{\pm}$ are related to integrals calculated in Ref. 25 through the relations

$$\frac{\partial \mathcal{R}_0^{\pm}}{\partial \omega} \equiv i\int_0^{\infty} (\Psi_0^{\pm})^2 r dr, \quad \frac{\partial \mathcal{R}_0^{\pm}}{\partial \mathrm{R}_m} \equiv i\bar{\mu}\int_0^{1} (\Psi_0^{\pm})^2 r dr. \tag{C5}$$

In the following, we shall focus on the case $\bar{\mu}=0$ and we introduce the notations

$$\frac{\partial \mathcal{F}_0}{\partial \bar{\mathrm{R}}_m} = -iC_0(f_1+if_2), \quad \frac{\partial \mathcal{F}_0}{\partial \bar{\omega}} = -iC_0(g_1+ig_2),$$
$$\frac{\beta_{-1}}{\mathcal{F}_{-1}} + \frac{\beta_{+1}}{\mathcal{F}_{+1}} = X+iY. \tag{C6}$$

Solutions of (C2) are

$$\mathrm{R}_2 = \left(\frac{\mathrm{R}_0}{4}\right)^2 \frac{Xg_1+Yg_2}{f_1g_2-f_2g_1}, \quad \omega_2 = \left(\frac{\mathrm{R}_0}{4}\right)^2 \frac{Xf_1+Yf_2}{f_1g_2-f_2g_1} \tag{C7}$$

recovering results similar to those obtained in Ref. 25 using a different approach.

We have in mind that for some values of ω_f, resonance can occur. An oscillating system forced at a resonant frequency is prone to instability and a large negative threshold shift is expected. However, inspection of (C7) reveals no clear relation between the sign of R_2 and the forcing frequency, which appears in the quantities X and Y. We only know that $f_1g_2-f_2g_1<0$, since near the critical point ($\delta R = \bar{\mathrm{R}}_m - \mathrm{R}_0$) the denominator in (C7) is proportional to the growth rate of the dynamo driven by a steady flow. When $\rho=0$, we shall consider Eq. (C2) for an imposed $\delta\mathrm{R}$ and complex values of $\delta\omega=\omega_1+i\sigma_1$, where ω_1 is the frequency shift and $\mathrm{Re}\,(\gamma)=-\sigma_1$ is the growth rate, given by

$$\sigma_1 = \delta\mathrm{R}\frac{f_1g_2-f_2g_1}{g_1^2+g_2^2}. \tag{C8}$$

Above the dynamo threshold ($\delta\mathrm{R}>0$) the field is amplified [$\mathrm{Re}\,(\gamma)>0$]; thus, $\sigma_1<0$ and $f_1g_2-f_2g_1<0$.

In the high frequency limit ($\omega_f \gg \omega_0$), expressions for X and Y can be derived explicitly using the asymptotic behavior of the Bessel functions for large arguments. For $\bar{\mu}=0$ with $q_{\pm1}=s_{\pm1}\approx(\omega_f\pm\omega_0)^{1/2}(1\pm i)/\sqrt{2}$ and using the asymptotic behavior, i.e., $\beta_{\pm1}/\mathcal{F}_{\pm1}\to(s_{\pm1})^{-3}$, one gets

$$X+iY = -\sqrt{2}\omega_f^{-3/2}\left(1-i\frac{3\omega_0}{2\omega_f}\right). \tag{C9}$$

When $\bar{\mu}=0$, we have also $f_1=1/2$ and $f_2=0$, leading to the expression for R_2:

$$\mathrm{R}_2 \approx -\frac{\mathrm{R}_0^2}{4\sqrt{2}}\omega_f^{-3/2}\left(\frac{g_1}{g_2}-\frac{3\omega_0}{2\omega_f}\right). \tag{C10}$$

For the wave numbers $m=-k=1$, numerical calculations of g_1 and g_2, which depend only on the critical parameters R_0 and ω_0, give $g_1/g_2=1.626$, and thus $\mathrm{R}_2<0$ when $\omega_f\to\infty$.

When $\bar{\mu}=0$, there are several reasons to consider the particular value of the forcing; i.e., $\omega_f=2\omega_0$. One of them is that for Hill or Mathieu equations it is a resonant frequency. Moreover, in the present problem it leads to simplified calculations. In particular the asymptotic behavior of $\beta_n/\mathcal{F}_n$ can still be used for $n=+1$ since $\omega_f+\omega_0$ is large, while the approximation is no longer valid for $n=-1$. Nevertheless, the mode $n=-1$ is remarkable since it corresponds to $s_{-1}=s_0^*$, from which it follows that $\beta_{-1}=\beta_0^*$ and $\mathcal{F}_{-1}=-i\mathrm{R}_0\beta_0^*$. Finally, one gets the exact result: $\beta_{-1}/\mathcal{F}_{-1}=i/\mathrm{R}_0$, which leads to

$$X+iY \approx \frac{i}{\mathrm{R}_0}+\frac{1}{s_1^3} \quad \text{with } s_1^3 \approx -2\left(\frac{3\omega_0}{2}\right)^{3/2}(1-i). \tag{C11}$$

For the values $\mathrm{R}_0=20.82$ and $\omega_0=4.35$ corresponding to Fig. 8(f), one gets $X=-1.5\times10^{-2}$ and $Y=3.3\times10^{-2}$. The threshold shift is

$$\mathrm{R}_2 \approx \frac{\mathrm{R}_0^2}{8}(1.62X+Y) = 0.48, \tag{C12}$$

showing that the sign of R_2 changes when ω_f decreases from infinity to $2\omega_0$. This result is in qualitative agreement with the exact results reported in Fig. 8(f), where $\mathrm{R}_2=0$ for $\omega_f=8.3\simeq2\omega_0$. When the forcing frequency is exactly twice the eigenfrequency ω_0, we had rather expected a large negative value of R_2 on the basis that it is a resonant condition for ordinary differential system under temporal modulation. In Fig. 8(f), the maximum negative value of R_2 occurs for $\omega_f\simeq4\omega_0$, which cannot be explained by simple arguments.

For $\bar{\mu}\neq0$, we have not been able to find resonant conditions such as: $n\omega_f+m\omega_0=0$ (n, m integers) between ω_f and ω_0 such that ω_f would be associated with a special behavior of the threshold shift. Contrary to the Hill equation, the induction equation is a partial differential equation with the consequence that the spatial and temporal properties of the dynamo are not independent. The wave numbers k and m are linked to the frequencies ω_0 and ω_f through $q_{\pm n}$ and $s_{\pm n}$, which appears as arguments of Bessel functions having rules of composition less trivial than trigonometric functions. Exhibiting resonant conditions implies to find relationship between $q_{\pm n}$, $s_{\pm n}$, and q_0, s_0 for specific values of ω_f. We have shown above for $\bar{\mu}=0$ that a relation of complex conjugation exists for $n=-1$ when $\omega_f=2\omega_0$, but we have not yet found how to generalize to other values of $\bar{\mu}$, and have left this part for a future work.

APPENDIX D: RESOLUTION OF CASE (II): SMOOTH FLOW

We define the trial functions $\psi_j^{\pm}=K_{m\pm1}(k)J_{m\pm1}(\alpha_j r)/J_{m\pm1}(\alpha_j)$, where the α_j are the roots of the equation

$$\alpha_j\left[\frac{K_{m+1}(k)}{J_{m+1}(\alpha_j)}-\frac{K_{m-1}(k)}{J_{m-1}(\alpha_j)}\right]+2k\frac{K_m(k)}{J_m(\alpha_j)}=0, \tag{D1}$$

and where J and K are, respectively, the Bessel functions of first kind and the modified Bessel functions of second kind. For $r\leq1$, we look for solutions in the form

$$b^{\pm} = \sum_{j=1}^{N} b^j(t)\psi_j^{\pm}(\alpha_j r), \tag{D2}$$

where N defines the degree of truncature. For $r\geq1$, the solutions of (10) are thus of the form

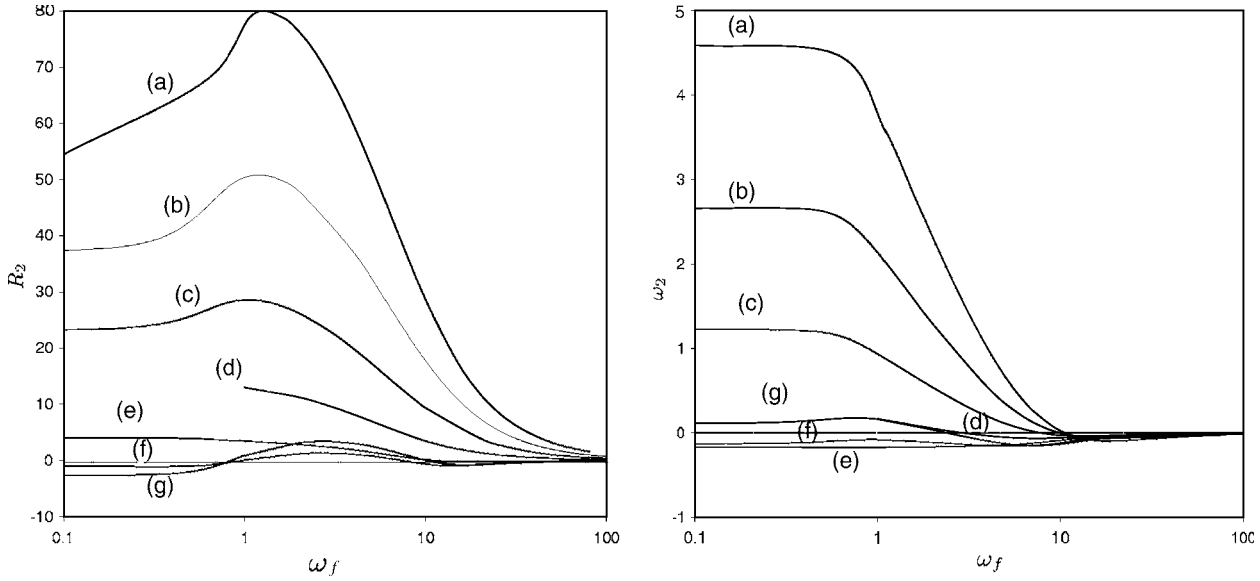

FIG. 7. Results obtained by the perturbative approach for $m=1$, $k=-0.56$, and $\bar{\mu}=0.44$ ($\bar{\Gamma}=1$). The dynamo threshold R_2 is plotted versus ω_f for several values of $\tilde{\mu}$= (a) 1.56; (b) 1.28; (c) 1; (d) 0.72; (e) 0.44; (f) 0.16; and (g) 0.

$$b^{\pm} = K_{m\pm1}(kr)\sum_{j=1}^{N} b^j(t) \tag{D3}$$

and, from (D1), these solutions satisfy the conditions (11) at the interface $r=1$. To determine the functions $b_j(t)$, it is sufficient to solve the induction equation (8) for $r\leq 1$. For that, we replace the expression of $b^{\pm}$ given by (D2) into the induction equation (8), in order to determine the residual

$$\mathrm{R}^{\pm} = \sum_{j=1}^{N} \{\dot{b}_j + [k^2+\alpha_j^2 + i(m\Omega + kV)]b_j\}\psi_j^{\pm} \mp \frac{i}{2} r\Omega' \sum_{j=1}^{N} b_j(\psi_j^+ + \psi_j^-). \tag{D4}$$

We then solve the following system:

$$\int_0^1 \mathrm{R}^+\phi_i^+ r dr + \int_0^1 \mathrm{R}^-\phi_i^- r dr = 0, \quad i=1,\ldots,N, \tag{D5}$$

where the weighting functions are defined by $\phi_j^{\pm} = J_{m\pm1}(\alpha_j r)/J_{m\pm1}(\alpha_j)$. Using the orthogonality relation

$$\int_0^1 \phi_i^+\psi_j^+ r dr + \int_0^1 \phi_i^-\psi_j^- r dr = \delta_{ij}G_{ij} \tag{D6}$$

with

$$G_{ii} = \frac{K_{m+1}(k)}{J_{m+1}^2(\alpha_i)}\int_0^1 J_{m+1}^2(\alpha_i r) r dr + \frac{K_{m-1}(k)}{J_{m-1}^2(\alpha_i)}\int_0^1 J_{m-1}^2(\alpha_i r) r dr, \tag{D7}$$

we write the system (D5) in the following matrix form:

$$\dot{\mathbf{X}} = M\mathbf{X} \quad \text{with } \mathbf{X} = (b_1,\ldots,b_N) \tag{D8}$$

with

$$M_{ij} = \delta_{ij}(k^2+\alpha_j^2) + \frac{i}{G_{ii}}\int_0^1 (\phi_i^+\psi_j^+ + \phi_i^-\psi_j^-)(m\Omega + kV) r dr - \frac{i}{2G_{ii}}\int_0^1 (\phi_i^+ - \phi_i^-)(\psi_j^+ + \psi_j^-)\Omega' r^2 dr. \tag{D9}$$

The numerical resolution of this system is done with a fourth-order Runge-Kutta time-step scheme. We took a white noise as an initial condition for the b_j.

APPENDIX E: ERRATUM OF NORMAND (2003) RESULTS (REF. 25)

For very small values of the fluctuation rate ρ and for an infinite shear [case (i)], a comparison can be made between the results obtained for $\tilde{\mu}=0$ by the method based on Floquet theory (see Appendix A) and those obtained by a perturbative approach,[25] which consists in expanding $\bar{\mathrm{R}}_m$ and the frequency $\mathrm{Im}(p)$ in powers of ρ according to

$$\mathrm{Im}(p) = \omega_0 + \rho\omega_1 + \rho^2\omega_2 + \cdots, \tag{E1}$$

$$\bar{\mathrm{R}}_m = \mathrm{R}_0 + \rho\mathrm{R}_1 + \rho^2\mathrm{R}_2 + \cdots, \tag{E2}$$

where R_0 and ω_0 are, respectively, the critical values of the Reynolds number and the frequency in the case of a stationary flow. At the leading order, it appears that $\omega_1=\mathrm{R}_1=0$. At the next order, the expressions of R_2 and ω_2 are given in Ref. 25; however, their numerical values are not correct due to an error in their computation.

After correction, the new values of R_2 and ω_2 are given in Fig. 7 for the set of parameters considered in Ref. 25: $m=1$, $k=-0.56$, and $\bar{\Gamma}=1$ ($\bar{\mu}=0.44$). The different curves correspond to values of $\tilde{\Gamma}$, which are not necessarily the same as those taken in Ref. 25. For $|\tilde{\mu}|$ sufficiently small (curves e and f), R_2 changes its sign twice versus the forcing frequency. We find that R_2 is negative for low and high frequen-

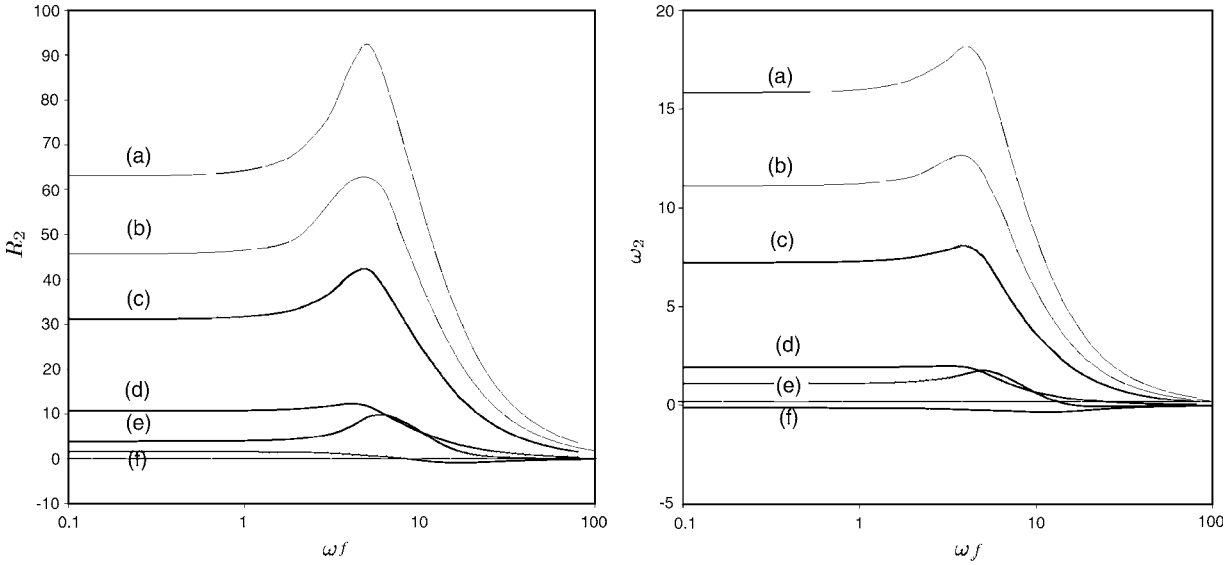

FIG. 8. Same as Fig. 7, but for $m=1$, $k=-1$, and $\bar{\mu}=0$ ($\bar{\Gamma}=1$). The labels correspond to $\tilde{\mu}$=(a) 1.5; (b) 1.25; (c) 1; (d) 0.5; (e) −0.5; and (f) 0.

cies, implying a dynamo threshold smaller than the one for the stationary flow. At intermediate frequencies, R_2 is positive with a maximum value, implying a dynamo threshold larger than the one for the stationary flow. For larger values of $|\tilde{\mu}|$ (curves a, b, c, and d) R_2 is positive for all forcing frequencies with a maximum value at a low frequency, which increases with $|\tilde{\mu}|$. This implies that for $|\tilde{\mu}|$ sufficiently large, the dynamo threshold is larger than the one obtained for the stationary flow, as was already mentioned in Sec. III A. For $\tilde{\Gamma}=1.78$, we have $\tilde{\mu}=0$. In this case, we have checked that the values of R_2 and ω_2 are in good agreement with the values of R_m and $\bar{\omega}$ obtained by the method of Appendix A, provided $\rho \leq 0.1$.

For completeness, we have also calculated the values of R_2 and ω_2 for $m=1$, $k=-1$, and $\bar{\Gamma}=1$, ($\bar{\mu}=0$), as considered in the body of the paper. The results are plotted in Fig. 8. Qualitatively, the results are in good agreement with those of Fig. 7. For $\tilde{\mu}=0$ again, we have checked that the values of R_2 and ω_2 are in good agreement with the values of R_m and $\bar{\omega}$ obtained by the method of Appendix A, provided $\rho \leq 0.1$. For higher values of the modulation amplitude ρ, the relative difference between the results obtained by the two methods can reach 10% on R_2 for $\rho=0.4$.

Finally, it must be noticed that our parameters $\tilde{\Gamma}$ and ω_f are strictly equivalent to, respectively, ε_1 and σ in Ref. 25.

[1] P. Cardin, D. Jault, H.-C. Nataf, and J.-P. Masson, "Towards a rapidly rotating liquid sodium dynamo experiment," Magnetohydrodynamics **38**, 177 (2002).
[2] M. Bourgoin, L. Marié, F. Pétrélis, C. Gasquet, A. Guigon, J.-B. Luciani, M. Moulin, F. Namer, J. Burgete, A. Chiffaudel, F. Daviaud, S. Fauve, P. Odier, and J.-F. Pinton, "Magnetohydrodynamics measurements in the von Karman sodium experiment," Phys. Fluids **14**, 3046 (2002).
[3] P. Frick, V. Noskov, S. Denisov, S. Khripchenko, D. Sokoloff, R. Stepanov, and A. Sukhanovsky, "Non-stationary screw flow in a toroidal channel: way to a laboratory dynamo experiment," Magnetohydrodynamics **38**, 143 (2002).
[4] F. Ravelet, A. Chiffaudel, F. Daviaud, and J. Léorat, "Towards an experimental von Karman dynamo: numerical studies for an optimized design," Phys. Fluids **17**, 117104 (2005).
[5] L. Marié, C. Normand, and F. Daviaud, "Galerkin analysis of kinematic dynamos in the von Kármán geometry," Phys. Fluids **18**, 017102 (2006).
[6] R. Avalos-Zunñiga and F. Plunian, "Influence of electro-magnetic boundary conditions onto the onset of dynamo action in laboratory experiments," Phys. Rev. E **68**, 066307 (2003).
[7] R. Avalos-Zunñiga and F. Plunian, "Influence of inner and outer walls electromagnetic properties on the onset of a stationary dynamo," Eur. Phys. J. B **47**, 127 (2005).
[8] N. Leprovost and B. Dubrulle, "The turbulent dynamo as an instability in a noisy medium," Eur. Phys. J. B **44**, 395 (2005).
[9] S. Fauve and F. Pétrélis, "Effect of turbulence on the onset and saturation of fluid dynamos," in *Peyresq Lectures on Nonlinear Phenomena*, edited by J. Sepulchre (World Scientific, Singapore, 2003), pp. 1–64.
[10] J-P. Laval, P. Blaineau, N. Leprovost, B. Dubrulle, and F. Daviaud, "Influence of turbulence on the dynamo threshold," Phys. Rev. Lett. **96**, 204503 (2006).
[11] F. Petrelis and S. Fauve, "Inhibition of the dynamo effect by phase fluctuations," Europhys. Lett. **76**, 602 (2006).
[12] F. Ravelet, "Bifurcations globales hydrodynamiques et magnétohydrodynamiques dans un écoulement de von Kármán turbulent," Ph.D. thesis, Ecole Polytechnique, Palaiseau, France, 2005.
[13] R. Volk, Ph. Odier, and J.-F. Pinton, "Fluctuation of magnetic induction in von Kármán swirling flows," Phys. Fluids **18**, 085105 (2006).
[14] D. Lortz, "Exact solutions of the hydromagnetic dynamo problem," Plasma Phys. **10**, 967 (1968).
[15] Yu. Ponomarenko, "Theory of the hydromagnetic generator," J. Appl. Mech. Tech. Phys. **14**, 775 (1973).
[16] P. H. Roberts, "Dynamo theory," in *Irreversible Phenomena and Dynamical Systems Analysis in Geosciences*, edited by C. Nicolis and G. Nicolis (D. Reidel, Dordrecht, 1987), pp. 73–133.
[17] A. D. Gilbert, "Fast dynamo action in the Ponomarenko dynamo," Geophys. Fluid Dyn. **44**, 241 (1988).
[18] A. A. Ruzmaikin, D. D. Sokoloff, and A. M. Shukurov, "Hydromagnetic screw dynamo," J. Fluid Mech. **197**, 39 (1988).
[19] A. Basu, "Screw dynamo and the generation of nonaxisymmetric magnetic fields," Phys. Rev. E **56**, 2869 (1997).
[20] A. D. Gilbert and Y. Ponty, "Slow Ponomarenko dynamos on stream surfaces," Geophys. Fluid Dyn. **93**, 55 (2000).
[21] A. D. Gilbert, "Dynamo theory," in *Handbook of MathematicalFluid Dynamics*, edited by S. Friedlander and D. Serre (Elsevier, New York, 2003), Vol. 2, pp. 355–441.
[22] A. Gailitis and Ya. Freiberg, "Non uniform model of a helical dynamo," Magnetohydrodynamics (N.Y.) **16**, 11 (1980).
[23] A. Gailitis, O. Lielausis, S. Dementiev, E. Platacis, A. Cifersons, G. Gerbeth, Th. Gundrum, F. Stefani, M. Christen, H. Hänel, and G. Will, "Detection of a flow induced magnetic field eigenmode in the Riga dynamo facility," Phys. Rev. Lett. **84**, 4365 (2000).

[24] A. Gailitis, O. Lielausis, E. Platacis, S. Dementiev, A. Cifersons, G. Gerbeth, Th. Gundrum, F. Stefani, M. Christen, and G. Will, "Magnetic field saturation in the Riga dynamo experiment," Phys. Rev. Lett. **86**, 3024 (2001).
[25] C. Normand, "Ponomarenko dynamo with time-periodic flow," Phys. Fluids **15**, 1606 (2003).
[26] A. A. Schekochihin, S. C. Cowley, J. L. Maron, and J. C. McWilliams, "Critical magnetic Prandtl number for small-scale dynamo," Phys. Rev. Lett. **92**, 054502 (2004).
[27] Y. Ponty, P. D. Mininni, H. Politano, J.-F. Pinton, and A. Pouquet, "Dynamo action at low magnetic Prandtl numbers: mean flow vs. fully turbulent motion," New J. Phys. (in press).
[28] A. A. Schekochihin, A. B. Iskakov, S. C. Cowley, J. McWilliams, M. R. E. Proctor, and T. A. Jousef, "Fluctuation dynamo and turbulent induction at low magnetic Prandtl numbers," New J. Phys. (in press); see also Fig. 2 of A. B. Iskakov, A. A. Schekochihin, S. C. Cowley, J. McWilliams, and M. R. E. Proctor, "Numerical demonstration of fluctuation dynamo at low magnetic Prandtl numbers," Phys. Rev. Lett. **98**, 208501 (2007).
[29] R. Monchaux, M. Berhanu, M. Bourgoin, P. Odier, M. Moulin, J.-F. Pinton, R. Volk, S. Fauve, N. Mordant, F. Pétrélis, A. Chiffaudel, F. Daviaud, B. Dubrulle, C. Gasquet, L. Marié, and F. Ravelet, "Generation of magnetic field by a turbulent flow of liquid sodium," Phys. Rev. Lett. **98**, 044502 (2007).